APPLICATION OF STRUCTURAL ENERGY STORAGE DEVICES IN AERIAL MONITORING SYSTEMS: A CONCEPTUAL DESIGN STUDY

D. Peyrow Hedayati[1], M. Kucher[1], H. Biggs[2], and R. Böhm[1]

[1] Faculty of Engineering, Leipzig University of Applied Sciences, Leipzig, Germany,
davood.peyrow_hedayati@htwk-leipzig.de
[2] National Institute of Water and Atmospheric Research (NIWA), Christchurch, New Zealand,
hamish.biggs@niwa.co.nz

Keywords: Multifunctional Energy Storage Composite (MESC); Structural Supercapacitor (SSC); Structural Battery (SB); Unmanned Aerial Vehicle (UAV)

ABSTRACT

Lightweight and energy-efficient structures are the cornerstones of new designs in demanding areas such as aerospace engineering. Electrically-powered Unmanned Aerial Vehicles (UAV) have widespread applications globally and are increasingly being used for high resolution surveying. However, on-board batteries typically make up to more than one third of a multi-rotor UAV's mass. In addition to their weight, the limited energy storage of batteries is another major problem for prolonged missions with higher payloads. Structural Electrical Energy Storage (EES) systems such as Structural Batteries (SB) and Structural Supercapacitors (SSC), also known as Multifunctional Energy Storage Composites (MESC), can potentially provide structural mass-saving and increased flight time. In this study, a concept for integrating the structural EES systems into Carbon Fibre Reinforced Polymer (CFRP) composite was introduced and its mechanical and electrical performance for a particular aerial surveying UAV use-case were investigated. In our concept design, the on-board batteries of the drone were replaced with a highly-integrated MESC. The design led to a weight reduction of 37.6% in the UAV. In addition, the introduction of the MESC did not depreciate the mechanical properties of the drone. Finally, the performance of the existing setup was compared against the concept configuration in a test mission simulation. The results show that highly-integrated MESCs can be successfully implemented in battery-less multi-rotor UAVs and improve their functionality by creating significant weight reduction.

1 INTRODUCTION

Unmanned Aerial Vehicles (UAV), commonly known as drones, are gaining more and more attention in many research applications because of their stability and relatively low cost [1]. For example, multi-rotor drones have enabled fast acquisition of high-resolution low-altitude aerial imaging in ecological studies [2] or on-site inspection of wind turbine blades [3]. Despite their practicality, several drawbacks hinder the full exploitation of UAVs. Most drones for civil applications use on-board batteries as their source of energy, with battery capacity limiting flight time, limiting flight range, and creating challenges for UAV mission planning [4]. In spite of the recent developments in material and manufacturing processes for conventional Li-ion batteries, the battery issue remains the greatest limiting factor in increased functionality of drones. A potential game-changer in the battery industry is the recent introduction of Structural Electrical Energy Storage (EES) or Multifunctional Energy Storage Composite (MESC). MESC combines the lightweight nature of Carbon Fibre Reinforced Polymers (CFRP) with an integrated battery function [5]. In this study, a conceptual design for integrating EES into the structural components of a popular multi-rotor drone, the DJI Matrice 600 Pro, was presented.

2 MULTIFUNCTIONAL ENERGY STORAGE COMPOSITES (MESC)

Multifunctionality in engineering concept is a holistic and multidisciplinary approach to optimize a system with respect to certain design drivers, e.g. weight and volume [6]. Multifunctional energy-storage devices can bear mechanical load while converting electrochemical energy at the same time [7]. Two important types of MESCs are Structural Batteries (SB) and Structural Supercapacitors (SSC). SB have the advantage of higher energy density, while SSC are maintenance-free and safe, offering higher power density and higher cyclic lifetime [8]. In this section, a brief overview of MESC applications is given. Various integration levels in a typical MESC are then discussed.

2.1 APPLICATIONS

MESC with integrated energy storage functionality is a relatively new field, which enables the possibility of platform-wide mass and volume reductions [9]. In 2004, NASA actualized the idea of a multifunctional structure that incorporates energy storage devices as load bearing elements in panel assemblies for application in a small-satellite (Fig. 1a) [10]. In another study, a structural battery is placed on the upper wing skin of a fixed-wing drone to increase the flight time (Fig. 1b) [11]. Additionally, in 2021, Tesla showcased the Model Y electric vehicle, which is powered by a structural battery pack with 4680 cells in the underbody of the car (Fig. 1c) [12]. The research for next-generation structural batteries is achieving new milestones. For example, a SB composite with remarkable multifunctional performance was developed by Asp et al., featuring an energy density of 24 Wh/kg, an elastic modulus of 25 GPa, and tensile strength exceeding 300 MPa (Fig. 1d) [13].

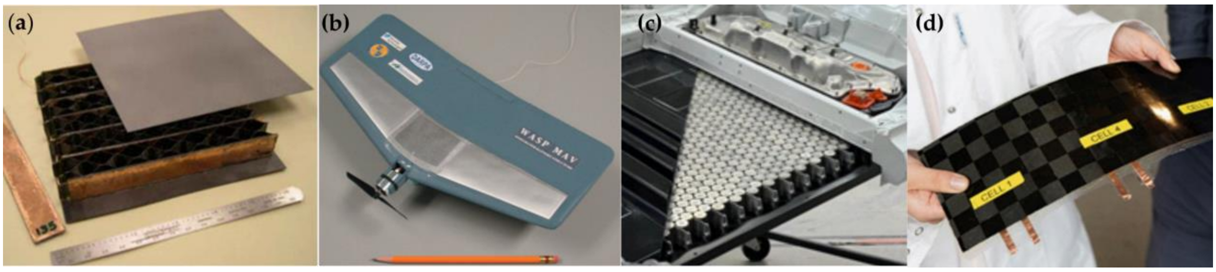

Figure 1: (a) A structural sandwich panel incorporating structural energy storage [10], (b) a micro drone with structural battery cells [11], (c) Tesla Model Y EV structural battery design [12], (d) a structural battery composite developed at Chalmers University of Technology [13].

Structural EES applications are not limited to SBs. The huge power density and the maintenance-free nature of supercapacitors make them an ideal choice for peak power applications. For example, a highly-integrated satellite panel structure was developed at the German Aerospace Center (DLR), which assembles several multifunctional panels into a single unit to obtain huge mass and volume savings [14]. The developed sandwich structure uses thin integrated SSC layers to power a vibration control system (Fig. 2).

2.2 INTEGRATION LEVEL

According to Adam's classification [15], there are essentially four Degrees of Integration (DoI) in MESCs. A functional separation or zero-integration level, DoI (0), refers to conventional non-load carrying battery setups. DoI (I), also referred to as integrated conventional storages, occurs when conventional batteries are placed into cavities or unused spaces in the structure. DoI (II) is achieved when thin film energy devices are integrated as interlayers into or onto the composite layers (Fig. 2). Creating energy storing capabilities at a meso scale, i.e. the actual laminates, represents a third-degree integration level, DoI (III). This is achieved by functionalizing individual single layers or constituents (Fig. 1d). DoI (III) is also known as single-ply functionalization (Fig. 3). As illustrated in Fig. 3, in the third-degree integration, a single layer of SB or SSC is placed within layers of carbon fibre reinforcements. The reinforcement layers made of conventional CFRPs are used for load-bearing purposes. Various fibre orientations and polymer matrices can also be used based on the requirements. The positive and negative electrodes in SB or SSC layers are made of carbon fibres. Unlike SSC, the positive electrode has a Li-metal doped coating in SB. The carbon fibres are placed within a Structural Battery Electrolyte (SBE) matrix. SBE is a specific polymer which is composed of two continuous phases: a solid polymer skeleton and a salt containing liquid electrolyte [25].

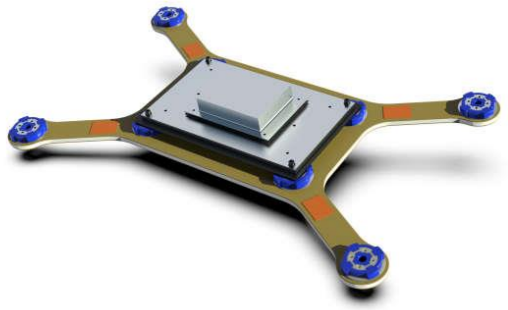

Figure 2: Multifunctional highly-integrated satellite panel powered by structural supercapacitors [14].

The highest possible integration level, DoI (IV), happens at a micro-scale (constituent functionalization). At this scale, single fibres are serving as both electrodes and reinforcements [16]. DoI (III) or embedded integration design is used in this study since it is widely investigated in the literature (see [13, 17, 18]).

2.3 MODELLING THE MULTIFUNCTIONAL PERFORMANCE

In this section, structural and electric efficiency metrics are introduced to assess the MESC's overall performance. First, the bending stiffness for a composite material is defined as a measure of its structural integrity. The electrical energy performance of structural EES is then evaluated.

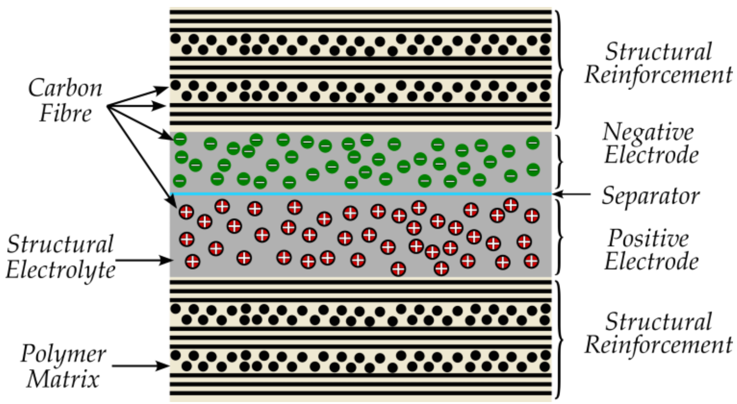

Figure 3: Schematic design of a multifunctional energy storage composite with a third-degree integration level (DoI (III)).

2.3.1 Structural Performance

In order to analyse the load-bearing capabilities of MESCs, the in-plane effective elastic moduli are conventionally used (see [13], for example). While effective moduli can give an accurate assessment of the laminated composite stiffness, it homogenizes the individual layer geometry [19]. This criterion becomes a drawback especially when structural parts need to be modified to integrate the EES modules (e.g. a change in layer thickness or total geometry). For this reason, a different metric is chosen which involves the bending stiffness of composite beams. In this way, the entire structure can be modeled as a beam at a preliminary level [19]. Composite beams are one of the fundamental structural components used in diverse lightweight applications. For example, in aerospace and drone engineering, composite beams are found in many areas (e.g. arms, legs, propellers, and chassis components) [20]. Therefore, it is rational to choose composite bending stiffness to assess the overall mechanical performance of multifunctional composites. Here, the Classical Laminate Theory (CLT) is employed to develop fundamental equations for the mechanics of laminated composite beams. According to CLT, the stiffness matrix composed of parameters A, B, and D relates the Cartesian components of force resultants (N_x, N_y, and N_z) and moment resultants (M_x, M_y, and M_z) to strains (ε_{0x}, ε_{0y}, and γ_{xy}) and curvatures (κ_x, κ_y, and κ_{xy}), as shown below,

$$\begin{bmatrix} N_x \\ N_y \\ N_z \\ M_x \\ M_y \\ M_z \end{bmatrix} = \begin{bmatrix} A_{11} & A_{12} & A_{16} & B_{11} & B_{12} & B_{16} \\ A_{12} & A_{22} & A_{26} & B_{12} & B_{22} & B_{26} \\ A_{16} & A_{26} & A_{66} & B_{16} & B_{26} & B_{66} \\ B_{11} & B_{12} & B_{16} & D_{11} & D_{12} & D_{16} \\ B_{12} & B_{22} & B_{26} & D_{12} & D_{22} & D_{26} \\ B_{16} & B_{26} & B_{66} & D_{16} & D_{26} & D_{66} \end{bmatrix} \begin{bmatrix} \varepsilon_{0x} \\ \varepsilon_{0y} \\ \gamma_{xy} \\ \kappa_x \\ \kappa_y \\ 2\kappa_{xy} \end{bmatrix}. \tag{1}$$

The above matrix is known as the ABD matrix. For a beam, parameters A, B, and D are given in the following equations [21],

$$A_{ij} = \sum_{k=1}^{N} b\bar{Q}_{ij}^{k}(h_k - h_{k-1}), \tag{2}$$

$$B_{ij} = \sum_{k=1}^{N} b\bar{Q}_{ij}^{k}\frac{({h_k}^2 - {h_{k-1}}^2)}{2}, \tag{3}$$

$$D_{ij} = \sum_{k=1}^{N} b\bar{Q}_{ij}^{k}\frac{({h_k}^3 - {h_{k-1}}^3)}{3}. \tag{4}$$

In equations (2), (3) and (4), b is the beam width, and h is the layers thickness. For the sake of simplicity, a one-dimensional analysis of the beam is performed according to the thin beam theory (also known as Classical Beam Theory (CBT)), in which effects of shear deformation and rotational inertia are neglected [19]. CBT is accurate for beams which have much smaller cross-sectional dimensions than beam lengths, as considered in the current study. Assumptions for these beams are that the normal to the beam mid-surface remain straight and normal. Both rotational inertia and shear deformation are neglected [19]. Thus, equation (1) is simplified as below,

$$\begin{bmatrix} N \\ M \end{bmatrix} = \begin{bmatrix} A_{11} & B_{11} \\ B_{11} & D_{11} \end{bmatrix} \begin{bmatrix} \varepsilon_0 \\ \kappa \end{bmatrix}, \tag{5}$$

where N and M are force and moment resultants in the x-direction. Similarly, ε_0 and κ are strains and curvatures at the middle surface in the x-direction. It should be noted that our simplification here has the downside of not considering any coupling. In order to resolve this problem, one can use the equivalent stiffness parameters that include coupling. To do so, matrix J is defined as the inverse of the ABD matrix [19],

$$J = \begin{bmatrix} A_{11} & B_{11} \\ B_{11} & D_{11} \end{bmatrix}^{-1}. \tag{6}$$

Using the matrix J, the equivalent modulus of elasticity and bending stiffness for the entire laminates can be defined as [19],

$$EI = \frac{1}{J_{22}}, \tag{7}$$

where J_{22} is the term in 2nd row and 2nd column of the J matrix and I is the moment of inertia.

2.3.2 Electrical Performance

The electrical performance of a conventional battery is given by its energy content (Γ_B),

$$\Gamma_B = CV, \tag{8}$$

where C is the capacity and V is the voltage at dielectric breakdown. Similarly, the energy content of a supercapacitor (Γ_{SC}) is given by the following equation,

$$\Gamma_{SC} = 0.5C_sV^2, \tag{9}$$

where C_s is the capacitance of the supercapacitor. In structural EES, it is common to use the mass specific values of energy content ($\bar{\Gamma}_B$ and $\bar{\Gamma}_{sc}$), which are defined in equations (10) and (11),

$$\bar{\Gamma}_B = \frac{\Gamma_B}{m_{SB}}, \tag{10}$$

$$\bar{\Gamma}_{sc} = \frac{\Gamma_{SC}}{m_{SC}}, \tag{11}$$

where m_{SB} and m_{SC} are the mass of the SB and SSC, respectively. Equations (10) and (11) are used to assess the electrical performance of the MESC used in the following use-case.

2.4 USE-CASE

2.4.1 INVESTIGATED UAV

The DJI Matrice 600 Pro is an appropriate use-case drone for the current concept study due to its wide applications in scientific and civil areas. Fig. 4 shows the different structural components of the drone and their corresponding mass percentages. The total battery modules in the drone weigh around 3.57 kg, which is 38% of the total drone mass. Moreover, the total mass of the structural components in the drone, which can potentially be replaced by MESC, is 3.75 kg.

From a configurational standpoint, structural components in the drone can be classified in two groups. First component group (C1) is a flat plate geometry and includes two center frames (CF) in the drone (Fig. 5a). The second component group (C2) refers to a cylindrical geometry and comprises tubular structures such as frame arms (FA), landing gear legs (LG), and landing skids (LS) (Fig. 5b,c). All components are made of bidirectional CFRP laminates, denoted as $(0/90)_s$, with a thickness of 1 mm. In the current design, the multirotor drone is powered with six modular on-board lithium-ion polymer (Li-PO) batteries (Model TB47S) [22].

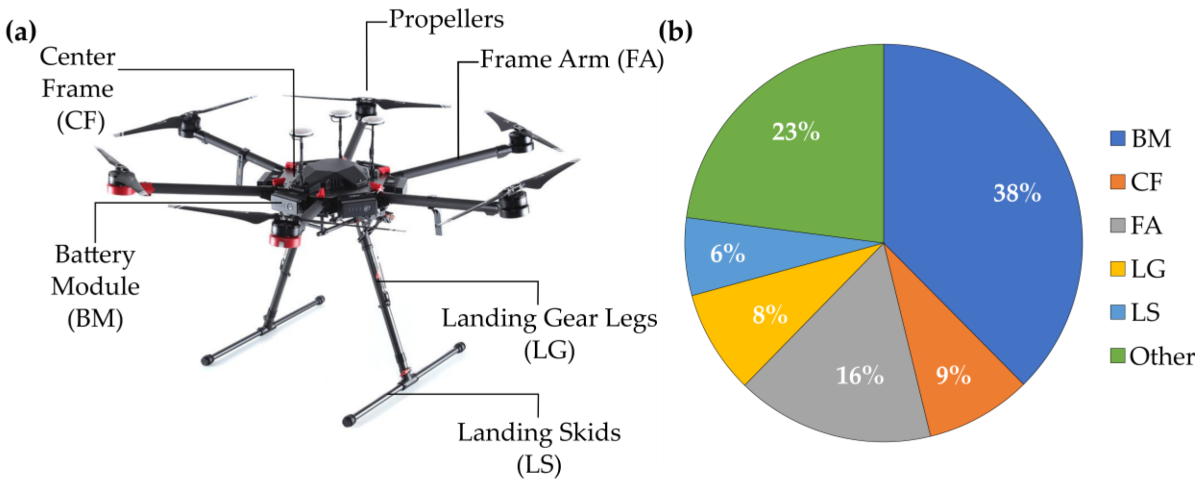

Figure 4: (a) Reference structural and battery components of the drone DJI Matrice (reproduced from [22]), and (b) the corresponding mass breakdown.

2.4.2 DESIGN CONCEPTS

The primary goal of the current design concept is to reduce the UAV mass by removing the on-board batteries and replacing the structural parts (C1 and C2) with MESC. For each component group in the structure, similar laminated composites could be used in different geometrical configurations (Fig. 6). MESCs with plate geometries are investigated by several researchers (see for example, [23–25]). On the other hand, tubular geometries are more challenging to manufacture and require more complex laminate designs. Therefore, few studies have been done on them. For example, Pyo et al. successfully manufactured a tubular supercapacitor with moderate electrochemical and mechanical performance [26].

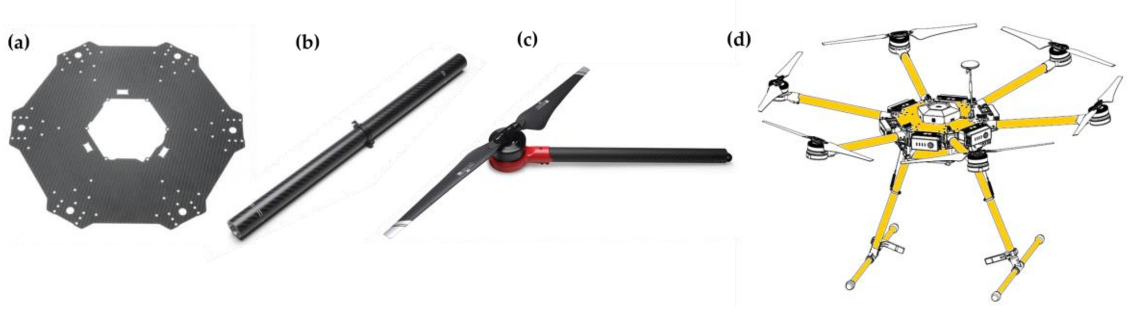

Figure 5: Structural CFRP components of DJI Matrice 600 Pro: (a) flat center frames, (b) landing gear legs, (c) frame arms, and (d) their position in the drone.

Following the framework suggested by Asp and Carlstedt [27], the concept design is presented using a SB MESC with DoI (III) (Fig. 3). A cross-sectional schematic of both component designs is shown in Fig. 6. In this design, positive and negative electrodes layers use unidirectional carbon fibre. The carbon fibres in the positive electrode are coated with Li-metal doped coatings. The polymer matrix in the SB layer is a SBE. At DoI (III), the polymer matrix in the reinforcement layers might be different from the SBE (Fig. 3). A thin polymer or glass fibre layer is used in the separator ply. Similar designs can be realized for supercapacitors with slight changes. For example, there is no need for a pouch cell layer in a supercapacitor and the carbon fibres in the positive electrode are not coated [28].

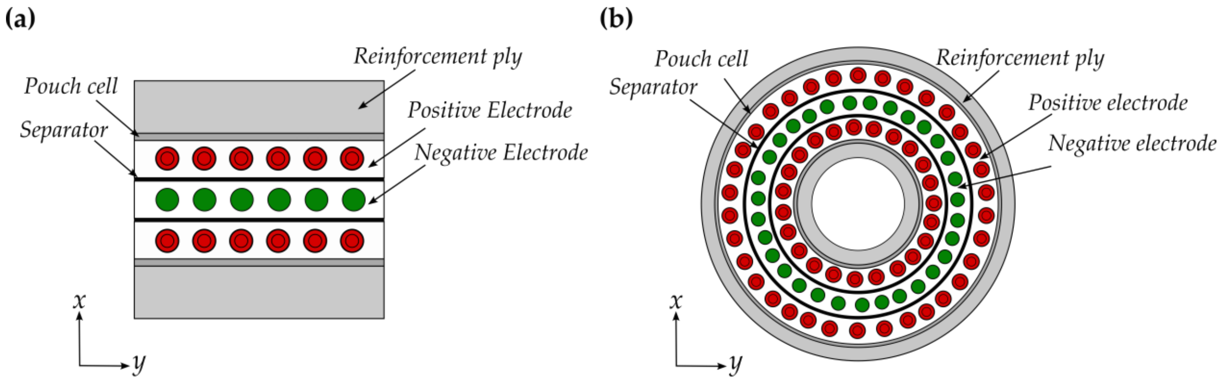

Figure 6: (a) Schematic design of structural battery for plate-shaped, and (b) tubular components.

3 RESULTS AND DISCUSSION

3.1 MULTIFUNCTIONALITY ANALYSIS

3.1.1 Structural Analysis

To conduct the structural analysis, C1 components in the drone are modelled as rectangular beams with a cross section area of 300 mm × 1.5 mm. Similarly, C2 components are modelled as tubular beams with the external radius 25 mm and internal radius 24 mm. The mechanical properties of the recommended MESC for the use-case are summarised in Table 1. Thereby the values of N, V_f, and t refer to the number of plies, volume fraction of the fibres, and the layer thickness, respectively. θ_1 and θ_2 refer to the orientation of each ply in the composite layers with respect to a reference axis. V_{Li} is the volume fraction of active materials (carbon fibres and $LiFePO_4$ particles). The properties of each layer are then summarized in Table 2.

Table 1: Composite lamina properties in the current and concept configuration.

Lamina	Current Design				Concept Design (MESC)				
	N	V_f	t (μm)	(θ_1/θ_2)	N	V_f	V_{Li}	t (μm)	(θ_1/θ_2)
Reinforcement ply	2	0.5	500	$(0/90)_s$	2	0.5	-	500	$(0/90)_s$
Pouch cell layer	-	-	-	-	2	-	-	70	-
Negative electrode	-	-	-	-	1	0.6	-	150	(0/0)
Separator	-	-	-	-	2	-	-	15	-
Positive electrode	-	-	-	-	2	0.6	0.35	75	(0/0)

Table 2: Layer properties of the plies used in the composite (data from [25, 27]).

Layer	Ply Thickness (μm)	Properties
Carbon fibre epoxy composite $V_f = 60\%$	500	E_L= 148 GPa; E_T = 9.65 GPa; G_{LT} = 4.55 GPa; $\nu_{LT} = 0.30$
Glass fibre woven lamina	70	$E_x = 19$ GPa; $E_y = 19$ GPa; $G_{xy} = 4.2$ GPa; $\nu_{xy} = 0.13$
Pouch bag lamina (isotropic)	70	$E = 1.5$ GPa; $G = 0.57$ GPa; $\nu = 0.32$
Structural battery composite with Whatman GF plain weave 0º/90º separator	330	$E_x = 25.4$ GPa; $E_y = 13.3$ GPa; $G_{xy} = 2.3$ GPa; $\nu_{xy} = 0.30$

Using equations (2)-(7) and the data provided in Tables 1 and 2, as well as the drone dimensions, the bending stiffness in the reference (current) design, EI_{ref}, and in the concept design EI_{concept}, can be calculated. The values of EI_{ref} and EI_{concept} for the drone are 0.943 Nm² and 3.87 Nm², respectively.

3.1.2 Electrical Analysis

Selection of the appropriate EES depends on the use-case requirements [29]. In practice, an ideal DoI (III) MESC incorporates an integrated EES layer with high energy density high mechanical property in all fibre directions. To date, there are only a few promising EES configurations reported with the features described. For example, the SB developed by Asp et al. [25] maintains an agreeable balance between mechanical performance and energy density. For this reason, the configuration in the work of Asp et al. [25] is used in our concept use-case. Key electrical properties in the current battery sets and the concept SB are summarized in Table 3. Using equations (8) and (10), and the data presented in Table 3, the total electrical energy of the on-board batteries in the current design Γ_{ref} and in the concept design $\Gamma_{\mathrm{concept}}$ of the drone are calculated as 420 Wh and 63 Wh, respectively.

Table 3: Electrical properties of the standard and structural battery used in the drone (data from [22] and [25]).

Property	Current Design	Concept Design	Unit
Specific capacity	7.56	8.55	Ah kg^{-1}
Nominal voltage during discharge	22.2	2.8	V
Max. calculated energy density	168	24	Wh kg^{-1}
*Total available effective energy**	420	63	Wh

*Effective energy is defined as 70% of the total available energy in the batteries.

3.1.3 Assessment of the multifunctional performance

According to Ashby's multi-objective optimization approach [30], the unitless multifunctional efficiency of a MESC η_{mf} depends on the relative electrical efficiency η_{e} and relative structural efficiency η_{s} [9]. This dependency is given by equation (12), as shown below,

$$\eta_{\mathrm{mf}} = \eta_e + \eta_s. \tag{12}$$

The relative electrical efficiency (η_{e}) is defined as the total electrical energy in the concept MESC $\Gamma_{\mathrm{concept}}$ divided by the total electrical energy available in the on-board batteries in the current reference drone design Γ_{ref},

$$\eta_e = \frac{\Gamma_{\mathrm{concept}}}{\Gamma_{\mathrm{ref}}}. \tag{13}$$

Similarly, the relative mechanical efficiency η_{s} is defined as the bending stiffness of the concept MESC, EI_{concept}, divided by the bending stiffness of the current reference drone design EI_{ref},

$$\eta_s = \frac{EI_{\mathrm{concept}}}{EI_{\mathrm{ref}}}. \tag{14}$$

According to Sections 3.1.1 and 3.1.2 and equations (13) and (14), the values for η_{e} and η_{s} are 0.15 and 4.10, respectively. Using equation (12), the multifunctional performance metric η_{mf} of the concept design of the drone is 4.25. According to O'Brien [31], a multifunctional system can provide system-wide mass saving when $\eta_{\mathrm{mf}} > 1$, which is the case in our concept.

On the other hand, minimising the structural weight in a drone increases the amount of payload that can be carried. Otherwise, if the weight reduction is not translated to payload, it reduces the energy consumption [32]. Weight reduction $\mathrm{WR}_{\%}$ in the concept drone can be calculated as below,

$$WR_{\%} = \left(1 - \frac{m_{SB}+m_{other}}{m_s+m_{other}+m_{BM}}\right) \times 100\%, \tag{15}$$

where m_{s} is the mass of the structural components, m_{BM} is the on-board Li-ion battery weight, m_{SB} is the mass of the structural battery, and m_{other} refers to the weight of non-energy and non-structural components (see Fig. 4). The data presented in Section 2.4.1 shows that a significant weight reduction in the concept design is achieved ($\mathrm{WR}_{\%}$= 37.6%). The relatively high value of $\mathrm{WR}_{\%}$ is the result of implementing the concept presented in this study, where C1 and C2 components in the drone are replaced with MESC and the on-board batteries are removed.

3.2 PERFORMANCE EVALUATION OF THE CONCEPT DRONE

To evaluate the practicality of our design, the performance of the concept drone against the current configuration of DJI Matrice 600 Pro drone is compared by simulating a mission. The selected test mission is done for river remote sensing using a hyperspectral camera to map toxic cyanobacteria [33]. However, the flight is simplified to only hovering, rather than translational motion, so that factors such as flight speed, wind speed, and others can be ignored. The multirotor drone is equipped with a camera payload of 4 kg and takes a time of 60 s to take off and ascend to an altitude of 120 m. It will then hover at that altitude for around 7 min and then takes 40 s to land and finally powers off. The energy used for this mission can be obtained using the model developed by Dorling [34]. Dorling's model estimates the amount of power needed for hovering a multi-rotor drone. According to this model, the power consumption is a linear function of the drone mass. The model assumes the absence of wind and wireless communication during the operation. The consumed power P according to Dorling model is given by [34],

$$P = \frac{(gm_T)^{\frac{3}{2}}}{\sqrt{2n\rho\xi}}. \tag{16}$$

In equation (16), g is the gravitational acceleration, m_T is the total drone mass, n is the number of rotors, ρ is the air density, and ξ is the propeller area. The amount of consumed energy required to perform the mission, U, can be obtained by integrating the power over mission duration t. This is given in the following equation,

$$U = \int_0^t P dt. \tag{17}$$

Fig. 7 shows the modelled power and energy consumption of the drone during a test mission based on equations (16) and (17). The solid and dotted yellow lines represent the required power P_{current} and the consumed energy U_{current} during the mission in the current drone design using on-board batteries. The solid and dotted black lines show the required power P_{concept} and consumed energy U_{concept} in the concept design using solely MESC as the source of electrical energy.

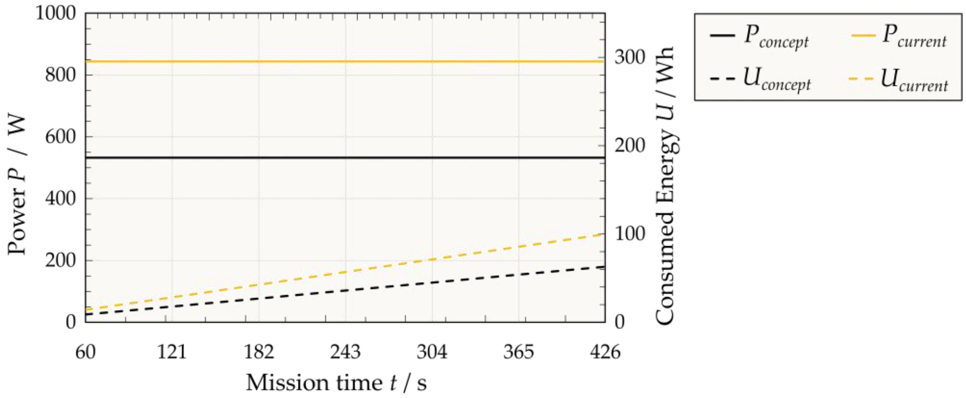

Figure 7: Power and energy consumption of the drone DJI Matrice 600 Pro during the hovering test mission using the current configuration (reference) and the concept (MESC) configuration.

As Fig. 7 suggests, for the same mission duration and payload, the concept design requires less power ($P_{\text{concept}} < P_{\text{current}}$) and less energy ($U_{\text{concept}} < U_{\text{current}}$) due to a significant weight reduction in the design. Moreover, according to Section 3.1.1, the recommended MESC possesses more bending stiffness than the current design. This means heavier payloads can be deployed, or the drone can fly better in turbulent windy conditions. It should be noted that the mission considered here is a simple one. More complex missions require longer durations and more energy, which surpasses the capabilities of the current EES systems. Therefore, it can be argued that although MESCs are successful in simple missions with moderate energy requirements, current EES cannot fully replace the existing battery systems. Table 4 summarises the key indicators of the drone concept design in this study.

Table 4: Key performance results in the concept MESC design for drone DJI Matrice Pro 600

Property	Value	Unit
Structural battery energy density	24	Wh kg^{-1}
Structural battery thickness	0.33	mm
Structural battery mass	3.57	kg
Multifunctional composite (MESC) thickness	1.5	mm
Multifunctional composite (MESC) bending stiffness	3.87	Nm^2
Multifunctional efficiency (η_{mf})	4.25	-
Weight reduction (WR%)	37.6	%
Max. hovering time of the concept drone with payload	430	s

3.3 CHALLENGES AND FUTURE WORK

The main consideration in designing MESCs is the choice of EES. While SBs provide satisfactory energy density, they lack high power density, high cyclability, and can potentially be dangerous in operation as a result of high fire hazard [35]. Although SSCs do not have most of the complications of SBs, they do have the key drawback of low energy density. For example, Mapleback et al. designed a SSC composite with an energy density of 2.64 Wh/kg and a corresponding shear strength of 71.5 MPa [18]. Higher energy densities are required for a complete replacement of on-board batteries with SSCs in a small UAV. A possible solution would be to combine SB and SSC composites, in particular where peak-power is required (see [14], for example). Nevertheless, given the special attention to SSCs in the research community, it seems that SSCs will make significant breakthroughs in the coming future [36]. In particular, electrode modifications via advanced porous carbon fibre, growth of vertically-aligned carbon nanotubes (VACNT), and carbon fibre functionalization [37] in combination with state-of-the-art additive manufacturing techniques are among recent efforts to gain high performing SSCs [38].

Another challenge in designing a MESC is to achieve synergistic and not parasitic combination of properties [15]. Degradation of EES performance under mechanical stress is an example of parasitic effect in MESCs. Similarly, charging or discharging of a EES composite will generate heat and as a result, the active electrode materials will expand or shrink. This volumetric change induces internal stresses within the material. The induced stress may cause mechanical and/or electrical failure [39].

On the other hand, charging a MESC may impose further challenges in practical applications. Replacing MESCs with another set will be expensive and challenging as the airframe protects delicate internal components, and it would not be practical to have to assemble/disassemble the aircraft between each flight. A potential solution is to use the wireless charging technology for drones [40].

Currently, drones are predominantly controlled by a human pilot, with swapping of batteries between flights being a straightforward procedure. However, fully autonomous drone operations are likely to increase in the future, where drones fly part of a specified mission, then return to a home base charging station (i.e. remote sensing, crop spraying, aerial deliveries, and many other applications). In these cases where swarms of drones are likely to be used, it makes more sense for drones to have integrated structural batteries, with the whole drone being recharged between flights. This will save significant weight by removing battery cases, battery attachment brackets, and other components on the drone. In these cases, MESCs are likely to be very useful and would be complementary to integrated batteries to increase energy density and mission flight time.

In conclusion, MESCs are likely to complement (or replace) the current battery technology in the future. Therefore, it is important to address technological and environmental aspects of MESCs in advance. For example, efficient manufacturing of MESC components and the appropriate selection of recycling strategies (for example, R^6-strategy [41]) are essential for the successful deployment of SBs and SSCs.

ACKNOWLEDGEMENTS

The research was funded by the M-Era.net project “Next Generation of 3D Printed Structural Supercapacitors” (PRINTCAP), Contract Number 100633785. This project is co-financed by public taxes from the budget approved by the Saxon State Parliament.

REFERENCES

[1] S. A. H. Mohsan, M. A. Khan, F. Noor, I. Ullah, and M. H. Alsharif, “Towards the Unmanned Aerial Vehicles (UAVs): A Comprehensive Review,” *Drones*, vol. 6, no. 6, p. 147, 2022.

[2] H. J. Biggs *et al.*, “Coupling Unmanned Aerial Vehicle (UAV) and hydraulic surveys to study the geometry and spatial distribution of aquatic macrophytes,” *Journal of Ecohydraulics*, vol. 3, no. 1, pp. 45–58, 2018, (doi: 10.1080/24705357.2018.1466666).

[3] A. S. Shihavuddin *et al.*, “Wind Turbine Surface Damage Detection by Deep Learning Aided Drone Inspection Analysis,” *Energies*, vol. 12, no. 4, p. 676, 2019, (doi: 10.3390/en12040676).

[4] H. J. Biggs, “Drone Flow User Guide v1.1 - River remote sensing and surface velocimetry,” National Institute of Water and Atmospheric Research (NIWA), Christchurch, New Zealand, Jun. 2022, (doi: 10.13140/RG.2.2.28299.77606).

[5] L. E. Asp, “Multifunctional composite materials for energy storage in structural load paths,” *Plastics, Rubber and Composites*, vol. 42, no. 4, pp. 144–149, 2013, (doi: 10.1179/1743289811Y.0000000043).

[6] M. A. Qidwai, J. Thomas, and P. Matic, “Structure-battery multifunctional composite design,” in 2002, pp. 180–191, (doi: 10.1117/12.475063).

[7] J. F. Snyder, E. L. Wong, and C. W. Hubbard, “Evaluation of Commercially Available Carbon Fibers, Fabrics, and Papers for Potential Use in Multifunctional Energy Storage Applications,” *J. Electrochem. Soc.*, vol. 156, no. 3, A215, 2009, (doi: 10.1149/1.3065070).

[8] M. Willuhn. “Massless’ battery breakthrough for lightweight EVs.” https://www.pv-magazine.com /2021/03/25/massless-battery-breakthrough-for-lightweight-evs/ (accessed Feb. 24, 2023).

[9] J. F. Snyder, D. J. O'Brien, and E. D. Wetzel, “Structural Batteries, Capacitors and Supercapacitors,” in *Handbook of solid-state batteries* (World Scientific series in materials and energy vol. 6), N. J. Dudney, W. C. West, and J. Nanda, Eds. New Jersey, London, Singapore, Beijing, Shanghai, Hong Kong, Taipei, Chennai, Tokyo: WORLD SCIENTIFIC, 2016, pp. 657–699.

[10] P. Lyman, J. Olson, and T. Feaver, “Application of Emerging Structural Energy Storage Technology to Small Satellite Systems,” in *18th Annual AIAA/USU Conference on Small Satellites*, 2004.

[11] J. P. Thomas and M. A. Qidwai, “The design and application of multifunctional structure-battery materials systems,” *JOM*, vol. 57, no. 3, pp. 18–24, 2005, (doi: 10.1007/s11837-005-0228-5).

[12] F. Lambert, “Tesla unveils new structural battery pack with 4680 cells in Gigafactory Berlin tour,” *Electrek.co*, 10 Oct., 2021. https://electrek.co/2021/10/10/tesla-unveils-new-structural-battery-pack-with-4680-cells-gigafactory-berlin/ (accessed: Feb. 24, 2023).

[13] J. Xu *et al.*, “A multicell structural battery composite laminate,” *EcoMat*, vol. 4, no. 3, e12180, 2022, (doi: 10.1002/eom2.12180).

[14] Z. Montano Rejas *et al.*, “Design and Manufacturing of a Multifunctional Highly Integrated Satellite Panel Structure,” in *ECSSMET 2021: the European Conference on Spacecraft Structures, Materials and Environmental Testing*, G. Aglietti, C. Bisagni, D. Boban, R. B. Dacal, G. Casarosa, and G. Coe, Eds., 2021.

[15] T. Adam *et al.*, “Multifunctional Composites for Future Energy Storage in Aerospace Structures,” *Energies*, vol. 11, no. 2, p. 335, 2018, (doi: 10.3390/en11020335).

[16] T. Carlson, *Multifunctional composite materials: Design, manufacture and experimental characterisation* (Doctoral thesis / Luleå University of Technology). Luleå: Luleå University of Technology, 2013.

[17] L. E. Asp, M. Johansson, G. Lindbergh, J. Xu, and D. Zenkert, “Structural battery composites: a review,” *Funct. Compos. Struct.*, vol. 1, no. 4, p. 42001, 2019, (doi: 10.1088/2631-6331/ab5571).

[18] B. Mapleback, V. Dao, L. Webb, and A. Rider, “Composite Structural Supercapacitors: High-Performance Carbon Nanotube Supercapacitors through Ionic Liquid Localisation,” *Nanomaterials*, vol. 12, no. 15, p. 2558, 2022, (doi: 10.3390/nano12152558).

[19] M. Hajianmaleki and M. S., “Mechanics of Composite Beams,” in *Advances in Composite Materials: Analysis of Natural and Man-Made Materials*.

[20] F. Turgut, A. Koycu, G. Neje, B. Behera, E. Ozden Yenigun, and H. Cebeci, “Hierarchical CNTs Grown Multifunctional 3D Woven Composite Beams for Aerospace Applications,” in *AIAA Scitech 2020 Forum*, Orlando, FL, 01062020, (doi: 10.2514/6.2020-0153).

[21] M. S. Qatu, *Vibration of laminated shells and plates*, 1st ed. Amsterdam, San Diego, CA: Elsevier, 2004.

[22] N. N. “DJI Matrice 600 Pro - DJI.” https://www.dji.com/de/matrice600-pro (accessed Feb. 24, 2023).

[23] K. Moyer *et al.*, “Carbon fiber reinforced structural lithium-ion battery composite: Multifunctional power integration for CubeSats,” *Energy Storage Materials*, vol. 24, pp. 676–681, 2020, (doi: 10.1016/j.ensm.2019.08.003).

[24] D. Carlstedt and L. E. Asp, “Performance analysis framework for structural battery composites in electric vehicles,” *Composites Part B: Engineering*, vol. 186, p. 107822, 2020, (doi: 10.1016/j.compositesb.2020.107822).

[25] L. E. Asp *et al.*, “A Structural Battery and its Multifunctional Performance,” *Adv Energy Sustain Res*, vol. 2, no. 3, p. 2000093, 2021, (doi: 10.1002/aesr.202000093).
[26] J. Pyo, H.-W. Park, M.-S. Jang, J.-S. Choi, S. K. Sathish Kumar, and C.-G. Kim, “Tubular laminated composite structural battery,” *Composites Science and Technology*, vol. 208, p. 108646, 2021, (doi: 10.1016/j.compscitech.2021.108646).
[27] D. Carlstedt, W. Johannisson, D. Zenkert, P. Linde, L. E. Asp, and (None), “Conceptual Design Framework for Laminated Structural Battery Composites,” in *ECCM18: 18th European Conference on Composite Materials*, Athens, Greece, I. M. Gullón, Ed., 2018.
[28] D. Peyrow Hedayati, G. Singh, M. Kucher, T. D. Keene, and R. Böhm, “Physicochemical Modeling of Electrochemical Impedance in Solid-State Supercapacitors,” *Materials*, vol. 16, no. 3, p. 1232, 2023, (doi: 10.3390/ma16031232).
[29] H. V. Abeywickrama, B. A. Jayawickrama, Y. He, and E. Dutkiewicz, “Comprehensive Energy Consumption Model for Unmanned Aerial Vehicles, Based on Empirical Studies of Battery Performance,” *IEEE Access*, vol. 6, pp. 58383–58394, 2018, (doi: 10.1109/ACCESS.2018.2875040).
[30] M. F. Ashby, “Multi-Objective Optimization in Material Design and Selection,” *Acta Metallurgica*, pp. 359–369, 2000.
[31] D. J. O'Brien, D. M. Baechle, and E. D. Wetzel, “Design and performance of multifunctional structural composite capacitors,” *Journal of Composite Materials*, vol. 45, no. 26, pp. 2797–2809, 2011, (doi: 10.1177/0021998311412207).
[32] C. Kassapoglou, *Design and analysis of composite structures: With applications to aerospace structures* (Aerospace series). Chichester West Sussex United Kingdom: John Wiley & Sons Inc, 2013.
[33] H. Biggs *et al.*, “Microcoleus Aerial Monitoring User Guide: Envirolink Tools Report,” Christchurch, New Zealand, 2021.
[34] K. Dorling, J. Heinrichs, G. G. Messier, and S. Magierowski, “Vehicle Routing Problems for Drone Delivery,” *IEEE Trans. Syst. Man Cybern, Syst.*, vol. 47, no. 1, pp. 70–85, 2017, (doi: 10.1109/TSMC.2016.2582745).
[35] J. A. Jeevarajan, T. Joshi, M. Parhizi, T. Rauhala, and D. Juarez-Robles, “Battery Hazards for Large Energy Storage Systems,” *ACS Energy Lett.*, vol. 7, no. 8, pp. 2725–2733, 2022, (doi: 10.1021/acsenergylett.2c01400).
[36] Y. Zhang *et al.*, “Excellent energy storage performance and thermal property of polymer-based composite induced by multifunctional one-dimensional nanofibers oriented in-plane direction,” *Nano Energy*, vol. 56, pp. 138–150, 2019, (doi: 10.1016/j.nanoen.2018.11.044).
[37] T. Boenke *et al.*, “Multi-functional carbon fibres for high-density energy storage in Lithium-Sulfur-batteries,” in *Carbon2018: The World Conference on Carbon*, Madrid, Spain, M. J. Lázaro, M. Á. Gilarranz, J. J. Rodriguez, F. Heras, and F. Carrasco, Eds., 2018.
[38] B. Karakashov *et al.*, “PRINTCAP: On the way to the new generation of 3D-printed structural supercaps,” in *23rd International Conference on Science and Applications of Nanotubes and Low-Dimensional Materials*, A. Loiseau and S. Maruyama, Eds., 2023.
[39] D. Carlstedt and L. E. Asp, “Thermal and diffusion induced stresses in a structural battery under galvanostatic cycling,” *Composites Science and Technology*, vol. 179, pp. 69–78, 2019, (doi: 10.1016/j.compscitech.2019.04.024).
[40] M. Lu, M. Bagheri, A. P. James, and T. Phung, “Wireless Charging Techniques for UAVs: A Review, Reconceptualization, and Extension,” *IEEE Access*, vol. 6, pp. 29865–29884, 2018, (doi: 10.1109/ACCESS.2018.2841376).
[41] P Johst, M Kucher, P Schulz, A Knorr, R Kupfer, R Böhm, “Identification of circular eco-subsystems for end-of-life aviation composite components based on a systematized R6-strategy,” in *12th EASN International Conference on Innovation in Aviation and Space for opening New Horizons*, Barcelona, Spain, J. Pons i Prats, A. Strohmayer, and S. Pantelakis, Eds., 2022.